J. Fluid Mech. (1981), *vol.* 102, *pp.* 329–352
Printed in Great Britain

Centrifugal instabilities during spin-down to rest in finite cylinders. Numerical experiments

By G. P. NEITZEL

Department of Mechanical and Energy Systems Engineering,
Arizona State University, Tempe, Arizona 85281

AND STEPHEN H. DAVIS

Department of Engineering Sciences and Applied Mathematics,
Northwestern University, Evanston, Illinois 60201

(Received 22 February 1980)

A cylinder filled with a viscous, incompressible fluid is in an initial state of rigid-body rotation about its axis of symmetry. If the container is brought to rest impulsively, the resulting unsteady spin-down flow may be subject to sidewall instabilities due to an imbalance between centrifugal and pressure gradient forces. These instabilities are examined numerically using a finite-difference simulation to integrate the axisymmetric Navier–Stokes equations for a variety of aspect ratios and Reynolds numbers. The Taylor–Görtler vortex-wavelength spectrum, the torque and the angular momentum histories are calculated. Criteria for the onset time for instability and the spin-down time are given. The effects of the enhanced mixing due to instability on the spin-down characteristics and torque are discussed. The results are compared with experiment.

1. Introduction

Consider an infinitely long circular cylinder of radius a filled with an incompressible fluid of kinematic viscosity ν. The system rotates as a solid body with rotation rate Ω about its axis of symmetry. At time $t' = 0$ the angular velocity of the cylinder is decreased impulsively to the value $\Omega - \Delta\Omega$. Due to the action of viscosity, an unsteady, pure-swirl flow is set up in which the only non-zero velocity component V is in the azimuthal direction and depends only on t' and the radial co-ordinate r'. The function V is the solution of a diffusion equation having diffusivity ν.

The shape of the instantaneous velocity profile of V, shown in figure 1, suggests on the basis of the Rayleigh criterion (Rayleigh 1916) that the swirl flow might be centrifugally unstable for early t' near $r' = a$. This criterion, however, is at most suggestive since it applies only to *steady* swirl flows of *inviscid* fluids. Here, the swirl is unsteady and viscously controlled. It would only be through experiment or direct calculation that instability could be determined.

Now consider the above situation for the completely enclosed geometry of a cylinder of length $2h$. Again, at $t' = 0$, the container has its angular velocity decreased from Ω to $\Omega - \Delta\Omega$. Again through viscous action, the fluid responds to the speed change by a process called *spin-down*. Because of the presence of the container end walls, there can no longer be a pure-swirl flow. The resulting flow will be unsteady and

0022-1120/81/4614-2800 $02.00

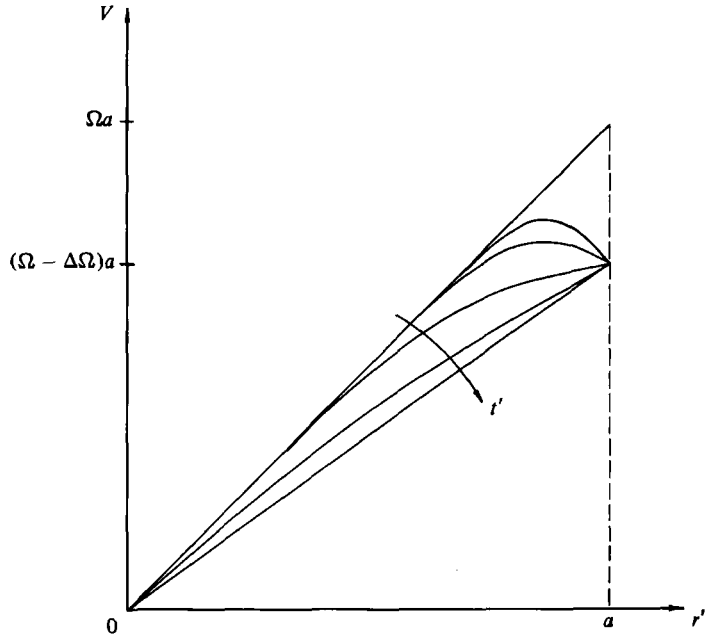

FIGURE 1. Azimuthal velocity profiles for impulsive spin decay within an infinite cylinder.

three-dimensional (though possibly axisymmetric). This flow is well understood in the limit $\Delta\Omega/\Omega \to 0$ as discussed by Greenspan & Howard (1963) for the case of $R = \Omega a^2/\nu \gg 1$. Here, for h/a not too large, the spin-down flow is dominated by Ekman 'blowing' into the interior by the Ekman boundary layers on the end walls. For the general case of $\Delta\Omega/\Omega$ not small, there is no analysis available since the spin-down flow is then strongly nonlinear.

The spin-down flow discussed above is axisymmetric and unsteady. For early times, however, the flow near the sidewalls should resemble the pure swirl discussed above for the case of an infinite cylinder. If such a flow is locally centrifugally unstable, then the whole manner of spin-down can be modified. To be sure, the Rayleigh criterion is an even more uncertain measure of instability here since, in addition to the basic state (spin-down) being unsteady and strongly influenced by viscosity, it is no longer a pure swirl flow. All the velocity components are necessarily non-zero. However, for the present case of finite cylinders we have direct evidence that spin-down can be centrifugally unstable and lead to the formation of axisymmetric vortices of Taylor–Görtler type.

Euteneuer (1969, 1970, 1972) used flow visualization to study the evolution of the wavelengths of such vortices during impulsive spin-down to rest for a variety of Reynolds numbers. The vortices constantly re-adjust to the increasing thickness of the side-wall layer. Euteneur plotted vortex wavelength λ/a *versus* Rayleigh-layer thickness $4(\nu t'/a^2)^{\frac{1}{2}}$ and fit the data for each Reynolds number with two straight line segments. The intersection of these two segments he called the 'Knickstelle', or 'knee point' and conjectured that its existence might be due to the appearance of Tollmien–Schlichting waves at the side wall. Michaelidis (1977) measured torque histories during impulsive spin-down to rest and correlated his results with those of

Euteneur. Tillmann (1967) looked at the onset of instability and transition to turbulence for a related problem employing two long concentric cylinders. At time zero the outer cylinder was impulsively stopped while the inner one continued to rotate with the initial angular velocity. Weidman (1976*b*) measured velocity profiles for non-impulsive spin-down using a laser-doppler velocimeter. Innes (1973) measured transient Ekman layer behaviour during impulsive spin-up and spin-down by monitoring thermistor beads at various radial positions on the cylinder end walls.

Theoretical and numerical work on spin-down has been limited. Euteneur, Heynatz & Siedenkersting (1968) computed azimuthal velocity profiles for spin-down using a modification of Wedemeyer's (1964) approach for spin-up and used these to estimate the effects of the end walls on the onset of the instability. Weidman (1976*a*) used a similar model for his computations for non-impulsive spin-down. Briley & Walls (1971) developed a finite-difference code to integrate the Navier–Stokes equations for spin-up and spin-down. In the latter case they present some streamline patterns for the vortices resulting from the centrifugal instability.

The initial motivation for this study came from observations on the dynamics of liquid-filled projectiles. The liquid payload of such a projectile is initially spun up in a nonlinear fashion as described by Wedemeyer (1964). At some point in the trajectory the payload reaches a state of near rigid-body rotation. However, the exterior of the projectile is acted upon by an aerodynamic roll-damping moment, so that subsequent to this spin-up time the liquid payload begins to spin down. If this spin-down is of sufficient magnitude to trigger instabilities in the sidewall boundary layer, then the modified torque on the projectile casing might lead to a gyroscopic and dynamic instability. In addition, instances of such unsteady swirl occur frequently in flows within turbomachines.

The object of the present work is the quantitative study of the instabilities during spin-down in finite circular cylinders. In particular, we shall concentrate on *spin-down to rest*. It is in this case that instabilities should be most prominent since here there is the greatest instantaneous, adverse distribution of angular momentum in the basic state. There are three features of the problem that are particularly noteworthy. (i) Spin-down to rest is a *strongly nonlinear process*. In the notation of our earlier discussion, $\Delta\Omega = \Omega$, so that no analytic expression is available for the basic state spin-down flow. (ii) The problem of instability of spin-down involves the examination of disturbances upon a three-dimensional, unsteady, viscous flow. This is a formidable task. (iii) More importantly, the problem itself is a *non-standard stability problem* in the following sense. Consider the sketch shown in figure 2. Here we graph from a 'thought' experiment the r.m.s. value of the disturbance (i.e. departure of the velocity from the spin-down basic state) velocity versus time. At $t' = 0$, the flow begins to spin down. The sidewall layer begins to thicken and at the onset time t_0 disturbances grow, perhaps to large amplitude. This large amplitude state contains the Taylor–Görtler vortices near the sidewalls, which enhance the mixing in the flow and perhaps greatly modify the rate of spin-down and the torque applied by the fluid to the container. These vortices then begin to fade away and after the spin-down time t_{sd} the fluid is again sensibly in solid body rotation. Unlike the standard instability which is a *permanent state*, the initial and final states (solid-body rotation) of our system are absolutely stable and hence the finite-amplitude instability is only a *transient*. In this sense spin-down instabilities are outside the realm of bifurcation theory (but see

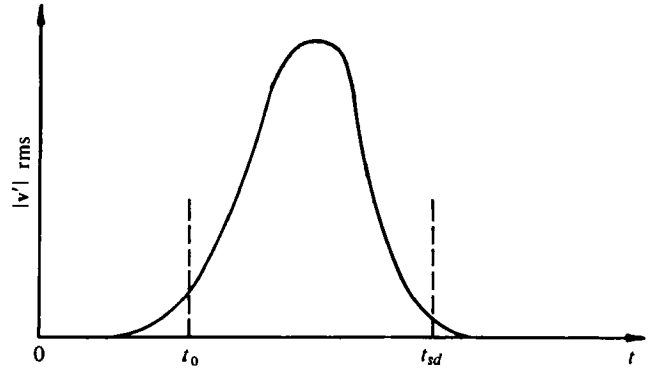

FIGURE 2. Hypothetical r.m.s. disturbance velocity *versus* time for spin-down.

Davis 1971). It is, though, possible to use energy stability theory to obtain lower bounds on t_0 and upper bounds on t_{sd} as Neitzel & Davis (1980) have for the case of pure swirl.

Since the basic state is strongly nonlinear and since we wish to describe a possibly large amplitude transient instability, we decided to use a direct numerical simulation of the flow field. We concentrate on the side-wall instabilities by examining only axisymmetric disturbances consistent with the common experimental observation (e.g. see Weidman 1976*b*) that such disturbances are the first observed. (Such a restriction, however, excludes any Ekman layer instabilities that might be present.)

We had available for use the finite-difference code of Kitchens (1980) that had been used successfully to simulate certain spin-up states. By appropriate modification axisymmetric spin-down instabilities could be examined. We aim at obtaining quantitative information on the flow fields, the modification by the instability of the rate of spin-down, and the torque exerted by the fluid on the container. It is the identification of the relevant time scales and the analysis of the mixing due to instability that is the main result of the present work.

2. Formulation

Consider a right circular cylinder of radius a and height $2h$ that is filled with an incompressible fluid of kinematic viscosity ν. For times $t' < 0$, the system rotates about its axis of symmetry with angular speed Ω and at $t' = 0$ the container is impulsively stopped.

The governing equations for the ensuing axisymmetric flow can be written in dimensionless form as follows:

$$\Gamma_t + \frac{1}{r}\psi_z\Gamma_r - \frac{1}{r}\psi_r\Gamma_z = \frac{1}{R}\left[\nabla_1^2\Gamma - \frac{1}{r}\Gamma_r\right], \tag{2.1a}$$

$$\zeta_t + \frac{1}{r}\psi_z\zeta_r - \frac{1}{r}\psi_r\zeta_z - \frac{u\zeta}{r} - \frac{2}{r^3}\Gamma\Gamma_z = \frac{1}{R}\left[\nabla_1^2\zeta + \frac{1}{r}\zeta_r - \frac{1}{r^2}\zeta\right], \tag{2.1b}$$

$$\nabla_1^2\psi - \frac{1}{r}\psi_r = r\zeta, \tag{2.1c}$$

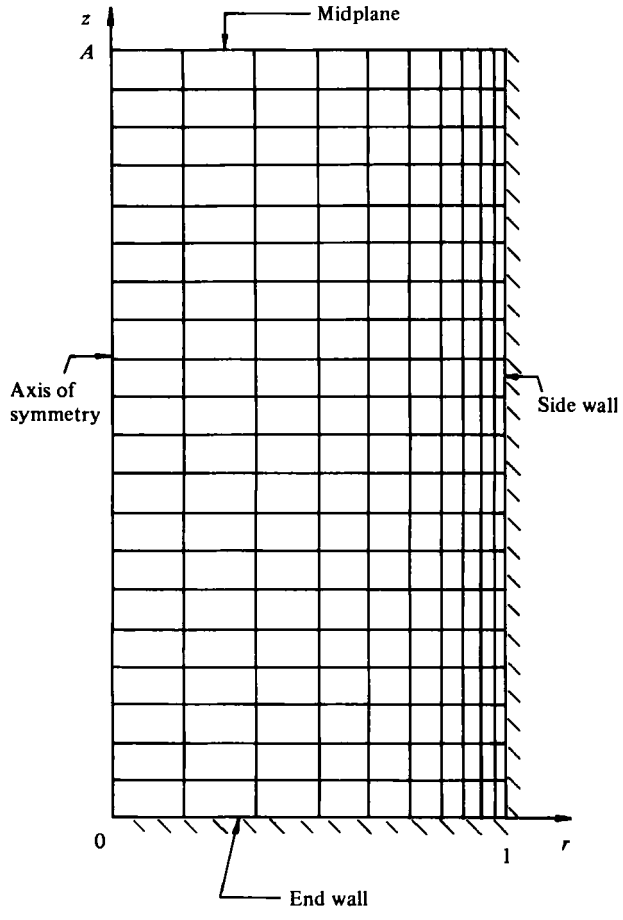

FIGURE 3. Typical computational grid (shown $\frac{1}{4}$ density) used for spin-down computations.

where

$$\nabla_1^2 = \frac{\partial^2}{\partial r^2} + \frac{\partial^2}{\partial z^2}. \tag{2.1d}$$

The velocity components are (u, v, w) in the directions given by the cylindrical coordinates (r, θ, z). Here the circulation is proportional to Γ,

$$\Gamma \equiv rv, \tag{2.1e}$$

the stream function ψ in the r, z plane is given by

$$u \equiv \frac{1}{r}\psi_z, \quad w \equiv -\frac{1}{r}\psi_r \tag{2.1f}$$

and ζ, the θ-component of vorticity, is given by

$$\zeta \equiv u_z - w_r. \tag{2.1g}$$

The variables have been made dimensionless using the following scales:

$$\text{speed} \to \Omega a; \quad \text{length} \to a; \quad \text{time} \to \Omega^{-1}. \tag{2.2}$$

The Reynolds number R is

$$R = \Omega a^2/\nu, \tag{2.3}$$

and the aspect ratio A is

$$A = h/a. \tag{2.4}$$

We further assume that the flow is symmetric about the midplane located at $z = A$. This allows us to reduce the size of the computational plane to half of what it would be otherwise, but restricts the number of disturbance vortices predicted to an even number. A sketch of the computational plane is given in figure 3.

Under the assumptions of axial and midplane symmetries, the boundary conditions for system (2.1) are as follows:

$$\text{at} \quad r = 0, \quad \psi = \Gamma = \zeta = 0; \tag{2.5a}$$

$$\text{at} \quad r = 1, \quad \psi = 0, \quad \Gamma = 0, \quad \zeta = \psi_{rr}; \tag{2.5b}$$

$$\text{at} \quad z = 0, \quad \psi = 0, \quad \Gamma = 0, \quad \zeta = \frac{1}{r}\psi_{zz}; \tag{2.5c}$$

$$\text{at} \quad z = A, \quad \psi = \Gamma_z = \zeta = 0. \tag{2.5d}$$

The initial condition is a state of rigid-body rotation. Therefore, we have

$$\text{for} \quad t < 0, \quad \psi = 0, \quad \Gamma = r, \quad \zeta = 0. \tag{2.6}$$

In order to resolve the side-wall boundary layer of the flow, a grid-stretching transformation is employed in the radial direction to place more grid points near the side wall than in the interior. The transformation is of the form

$$\hat{r} = \ln\left(\frac{b+r}{b-r}\right) \Big/ \ln\left(\frac{b+1}{b-1}\right), \tag{2.7a}$$

where

$$b = (1-q)^{-\frac{1}{2}}, \quad q < 1, \tag{2.7b}$$

and q is the user-selected constant which defines the amount of stretching. A similar stretching could be used in the z direction but technical considerations made this inconvenient. This is discussed more fully later.

Equations (2.1) and boundary and initial conditions (2.5) and (2.6) are expressed in terms of these new variables and the difference equations are then constructed from these using second-order-accurate expressions. For details the reader is referred to Neitzel (1979).

The ψ equation is solved by the Gauss–Seidel method of successive substitution, and the Γ and ζ equations are solved by the predictor–corrector multiple-iteration (PCMI) technique. Initial guesses for ψ, ζ, and Γ at the beginning of a new time step are extrapolated from the values at the three previous time steps, when these are available. Using these guesses, ψ_{zz} and ψ_{rr} are computed along $z = 0$ and $\hat{r} = 1$, respectively, to provide boundary data for ζ. One iteration of the PCMI technique is then performed. This begins at one row below the midplane ($z = A$), and solves the ζ and Γ equations for a single row implicitly. This is done for each row of points between the midplane and the end wall ($z = 0$). When this iteration has been completed, the ψ equation is solved iteratively to within some given tolerance, new boundary data are computed for ζ, and another iteration of the PCMI technique is performed. This process is

repeated until the values of ζ and Γ for a given iteration are within some given tolerance of their values for the previous iteration at every grid point. The user specifies a maximum number of iterations to be performed for ψ and for ζ and Γ. If the program performs this many iterations without converging, a warning message is printed and the computation proceeds using the values from the final iteration. It has been determined from numerous spin-up calculations that an occasional failure to converge does not qualitatively change the results. The program converges most slowly for ζ in the vicinity of the corner where the end wall and side wall meet. For the computations performed here, ten iterations were allowed for the ψ equation, and twenty-five iterations for the Γ and ζ equations.

There were no external disturbances imposed to trigger instability. The round-off and truncation errors were sufficient to give rise to Taylor–Görtler vortices, these errors presumably constituting small disturbances.

Briley & Walls (1971) treated similarly the problems of spin-up and spin-down, but employed the alternating-direction implicit (ADI) scheme and did not make use of either midplane symmetry or grid-stretching transformations. The PCMI procedure represents a compromise between explicit and fully implicit methods and is, in general, less time consuming than the latter. The use of equally spaced grid points imposes (for a given number of points) a restriction on the maximum Reynolds number for accurate computation, since the boundary-layer nature of the flow must be adequately resolved and these boundary layers decrease in thickness with increasing Reynolds number. For the case of impulsive *spin-up* from rest, Kitchens (1980) has been able to compute accurately the flow within a cylinder of aspect ratio unity for values of R as high as 50000. For a discussion of accuracy and stability of the method the reader is referred to Kitchens (1980).

3. Flow measures

Given a computation of a spin-down flow, one can judge to some extent the effects of instability, if any, by examining streamline contours. However, in order to gain a quantitative picture of the instabilities, other quantities must be defined and examined.

(*a*) *Torque.* The torque exerted by the fluid on the container is an experimentally measurable quantity. In fact it is from the torque data that many workers on Taylor vortices between rotating cylinders determine the onset of instability of Couette flow. Furthermore, the torque is a quantity of direct relevance to the dynamic stability behaviour of a liquid-filled projectile. The torque on the cylinder for the case of impulsive spin-down to rest has been measured for various Reynolds numbers by Michaelidis (1977). Comparison of the computational results with his data will be given later.

The total torque T on the cylinder may be separated into end-wall and side-wall components. This is a useful decomposition since the container aspect ratio is a parameter which influences the rate of spin-down, and the relative contributions of each component will vary with the aspect ratio. Also of interest is the way each of these components will be affected by the onset of instability. An increase in side-wall torque is expected following the appearance of Taylor vortices, but it is also possible that end-wall contributions may change, especially if a vortex forms near the corner.

The torque contributions are obtained by integrating the product of radius and

azimuthal stress component over the appropriate surfaces. The side-wall torque is given by

$$T_s = \frac{4\pi}{R}\int_0^A \left[\frac{\partial v}{\partial r} - \frac{v}{r}\right]_{r=1} dz, \tag{3.1}$$

and the end-wall component is given by

$$T_e = \frac{4\pi}{R}\int_0^1 r^2 \left[\frac{\partial v}{\partial z}\right]_{z=0} dr, \tag{3.2}$$

where the s and e subscripts designate side wall and end wall, respectively, stress has been scaled with $\rho\Omega^2 a^2$ and symmetry assumptions have been employed. Equations (3.1) and (3.2) are expressed in terms of second-order-accurate difference expressions in terms of Γ, $\hat{r}$, and z and the integrals evaluated by the trapezoidal rule. They are computed for each time step so that a time history of torque can be calculated.

(*b*) *Angular-momentum ratio.* The volume-integrated angular momentum ratio of the fluid within the cylinder is given by

$$L = 4\int_0^A \int_0^1 r^2 v \, dr \, dz, \tag{3.3}$$

scaled in units of the initial value $\pi\rho\Omega h a^4$. L is evaluated in terms of Γ, $\hat{r}$ and z using trapezoidal rule integration and obtained as a function of time.

The ratio L is of interest in determining the spin-down time, which we define to be that time t_{sd} at which the angular momentum L is e^{-1} of its initial value. The onset of Taylor–Görtler vortices should produce a noticeable effect on the angular momentum decay, since the vortices are effective in transporting higher angular momentum fluid from the interior to the region near the wall and because the velocity gradients within these vortices dissipate energy.

(*c*) *Rayleigh discriminant and Rayleigh length.* The Rayleigh criterion states that a necessary and sufficient condition for a *steady, inviscid, pure swirl flow* $V(r)$ to be linearly stable is that the inequality

$$\Phi(r) \equiv \frac{1}{r^3}\frac{d}{dr}|rV(r)|^2 > 0, \tag{3.4}$$

be satisfied for all r. The quantity $\Phi(r)$ is called the Rayleigh discriminant. Since the Rayleigh criterion is based on the assumption that the fluid is inviscid, and since viscosity is presumably a stabilizing influence for such swirl flows, a velocity profile which is predicted to be unstable on the basis of the Rayleigh criterion may indeed be stable in practice due to the effect of viscosity.

For spin-down within a finite cylinder, the flow is not only unsteady and viscous, but three-dimensional as well. From preliminary computations, it appears that the instability begins to form at the cylinder midplane and eventually propagates outward toward the end walls. On the basis of these computations, it was decided to calculate the Rayleigh discriminant as a function of radius and time at the container midplane. In addition, we were interested in what portion of the flow field at the midplane is 'potentially unstable' according to the Rayleigh criterion. Figure 4 is a sample plot of Φ versus r for a particular case considered. Φ is positive for all r up to about $r = 0{\cdot}9$, at which point it goes negative. We define the *Rayleigh length*, L_R, to be

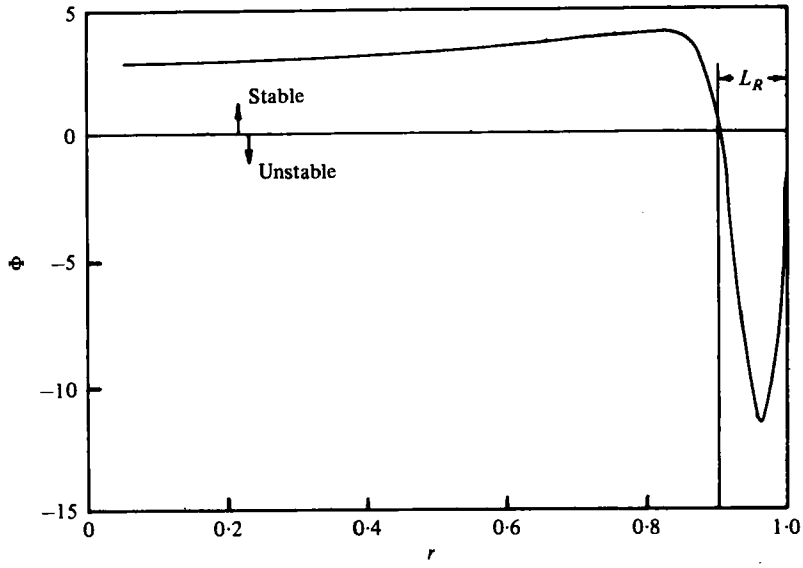

FIGURE 4. Rayleigh discriminant *versus* radius for impulsive spin-down to rest with $R = 2000$, $A = 1{\cdot}0$, $t_{bl} = 0{\cdot}141$.

the distance between the point at which Φ first crosses zero and the container side wall. For the above example, $L_R \approx 0{\cdot}1$. This quantity is computed as a function of time.

(*d*) *Spectral analysis and computational limitations.* As mentioned in the introduction, the experiments of Euteneur (1969, 1970, 1972) were concerned primarily with measurement of the time history of vortex wavelengths for the case of impulsive spin-down to rest. The vortices were made visible using aluminium flakes and axial wavelengths were determined from photographs. An average wavelength was calculated by dividing the axial length covered by the instability by the number of vortex pairs observed. Calculations of this type are possible in our computation from a visual inspection of the streamlines.

Inspection of streamline plots from preliminary computations indicates that there is no unique vortex wavelength, but rather a range of wavelengths at any given time. Because of this fact, it was decided that only a spectral analysis would be able to give quantitative information on the wavelength distribution of the vortex structure.

The discrete, one-dimensional Fourier transform $\Psi(k)$ of stream function $\psi(j)$ is defined by

$$\Psi(k) = \frac{2}{n}\sum_{j=0}^{n-1} \psi(j) e^{-2\pi i jk/n}, \quad k = 0, 1, \ldots, \frac{n-1}{2}, \tag{3.5}$$

where n is the number of data points and $i \equiv \sqrt{-1}$. The corresponding amplitude spectrum is defined by

$$A(k) = [\Psi(k)\bar{\Psi}(k)]^{\frac{1}{2}}, \quad k = 0, 1, \ldots, \frac{n-1}{2}, \tag{3.6}$$

where the overbar denotes complex conjugate. This *amplitude spectrum for the stream function* is computed at user-chosen radial positions by first calculating the values of ψ between the cylinder midplane and the top (from mirror symmetry considerations),

using a fast Fourier transform to compute $\Psi(k)$, and then calculating $A(k)$ from (3.6). These spectra may be plotted in histogram form at any radial position for any time.

It must be remarked that the decision to perform an axial spectral analysis using existing software (and equation (3.5)) necessitates either choosing a grid which is equally spaced in the axial direction, or interpolating to obtain equally spaced axial data. The latter choice yields spectra which are coloured by the interpolation scheme, while the former rules out the possibility of employing axial grid transformations to place more points in the Ekman layer on the cylinder end wall. The discussion in subsection (*c*) pointed out that the most critical location was the cylinder midplane, and that, after the initial formation at that location, the instability was propagated outward toward the end walls. This implies that good resolution is needed near the side wall along the entire length of the cylinder. This fact, when coupled with the need for equally spaced data for the spectral analysis, influenced the decision to use equally spaced axial grid points for all computations. Grid-stretching transformations were employed in the radial direction only.

A typical grid (shown $\frac{1}{4}$ density) which was used for the case of $R = 2000$, $A = 2{\cdot}0$ is shown in figure 3. The radial stretching here corresponds to a value of $q = 0{\cdot}1$ in equation (2.7).

This use of equally spaced axial grid points becomes a problem when trying to accurately compute high Reynolds number/high aspect ratio cases. Since the Ekman layer has thickness $O((A^2R)^{-\frac{1}{2}})$, we need to decrease the axial spacing when going to high R in order to maintain the needed resolution in this layer. Since computation time and storage are both expensive, we eventually reach a practical limit. For the computations done here, this practical limit on storage corresponds roughly to 41×81 grid, determined by memory restrictions for interactive processing.

(*e*) *Time scales.* The properties of spin-down and spin-down instabilities can be interpreted in terms of various time scales. We shall define these here in terms of the dimensional time t' and relate one to another.

The *radial-diffusion* time scale is given by

$$t_d = \nu t'/a^2. \tag{3.7}$$

The time scale associated with the impulsively generated side-wall (Rayleigh) *boundary layer* is given by

$$t_{bl} = 4(\nu t')^{\frac{1}{2}}/a, \tag{3.8}$$

which is the form used by Euteneuer to correlate his data.

Finally, there is the *Ekman* time scale associated with small Rossby number spin-up and spin-down by Greenspan & Howard (1963). This is given by

$$t_E = \Omega t' A^{-1} R^{-\frac{1}{2}}. \tag{3.9}$$

These time scales can be related to each other as follows:

$$t_{bl} = 4t_d^{\frac{1}{2}}, \tag{3.10a}$$

and

$$t_E = A^{-1}R^{\frac{1}{2}}t_d. \tag{3.10b}$$

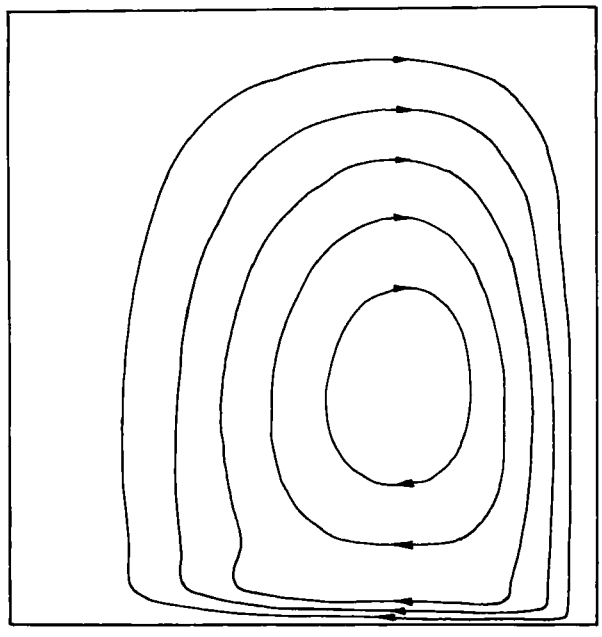

FIGURE 5. Instantaneous streamlines for case 5 ($R = 4000$, $A = 1{\cdot}0$) at $t_{bl} = 0{\cdot}100$.

4. Results and conclusions

The computations described in the previous sections have been performed for a variety of spin-down cases using a Control Data Corporation Cyber 70/76 with a Cyber 170/173 front end. Output from the Cyber 70/76 was stored on a disc drive unit attached to the Cyber 170/173 and subsequently analysed in an interactive graphics mode using a Tektronix 4014 terminal with PLOT 10 software.

Computations were performed for various Reynolds numbers and aspect ratios. The bulk of the computations were for the case of impulsive spin-down to rest since this case is most prone to instability and the experimental data of Euteneuer (1972) are available for comparison. A few non-impulsive cases were examined (Neitzel 1979) but these will not be discussed here.

Before we begin our discussion, let us reiterate the assumptions inherent in the numerical experiment. All flow quantities are assumed to be axisymmetric as well as symmetric about the midplane. Thus non-axisymmetric centrifugal instabilities are forbidden. Furthermore, an Ekman layer itself might be prone to instabilities but, since these are also non-axisymmetric, they are excluded as well. Only even numbers of axisymmetric vortices are examined. No external disturbances are imposed upon the flow in an attempt to induce certain modes of instability so that all instabilities grow from small disturbances to the flow due to round-off and truncation errors alone.

Let us consider a single case first, $R = 4000$, $A = 1$. This is later called case 5. Figures 5–9 show the instantaneous streamlines for times $t_{bl} = 0{\cdot}100$, $0{\cdot}187$, $0{\cdot}212$, $0{\cdot}264$ and $0{\cdot}346$. The boundaries of these streamline plots correspond to the boundaries of the computational plane given in figure 3 in which the bottom of each plot represents the end wall, the top is the midplane, and the left- and right-hand sides are the axis of

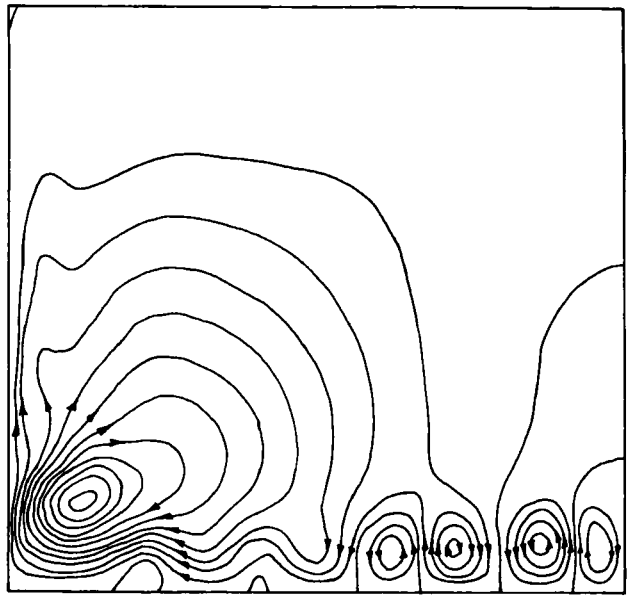

FIGURE 6. Instantaneous streamlines for case 5 ($R = 4000$, $A = 1{\cdot}0$) at $t_{bl} = 0{\cdot}187$.

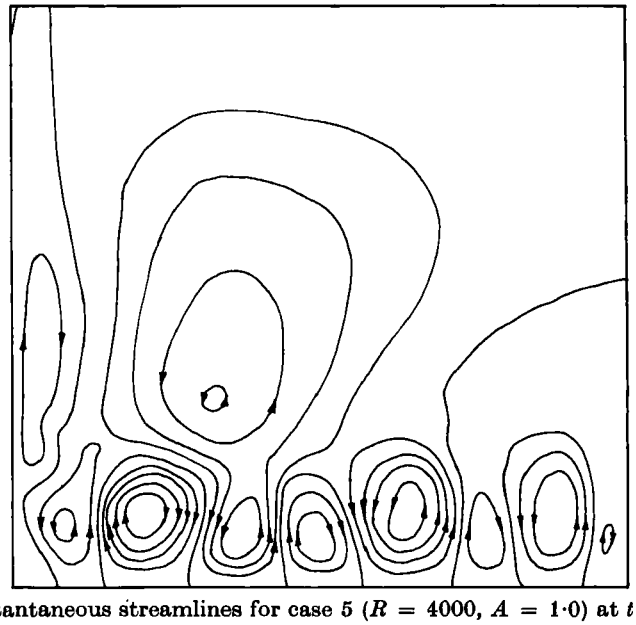

FIGURE 7. Instantaneous streamlines for case 5 ($R = 4000$, $A = 1{\cdot}0$) at $t_{bl} = 0{\cdot}212$.

symmetry and side wall, respectively. The entire flow field is represented by each figure plus its reflection across the midplane. For the infinite cylinder case, there is pure diffusion so that the 'spin-down' time should be $t_d = O(1)$ and hence $t_{bl} = O(1)$. Figure 5 shows the streamline pattern shortly after the cylinder has been stopped. The cellular pattern due to the Ekman layers is as yet undisturbed. In figure 6 we see the

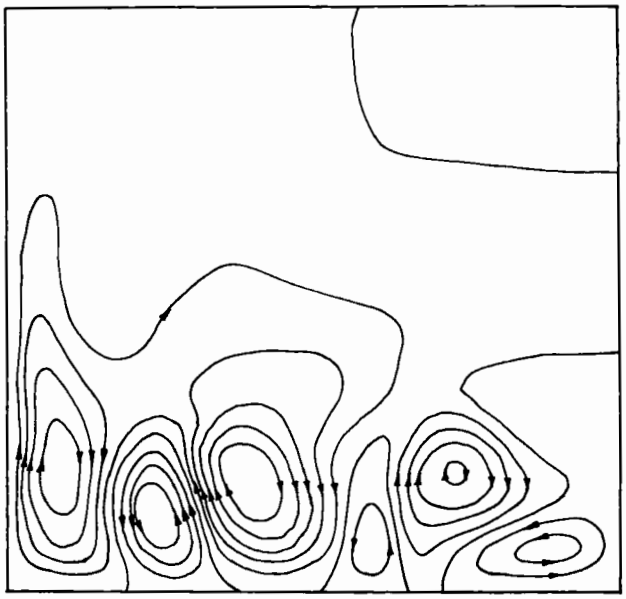

FIGURE 8. Instantaneous streamlines for case 5 ($R = 4000$, $A = 1{\cdot}0$) at $t_{bl} = 0{\cdot}264$.

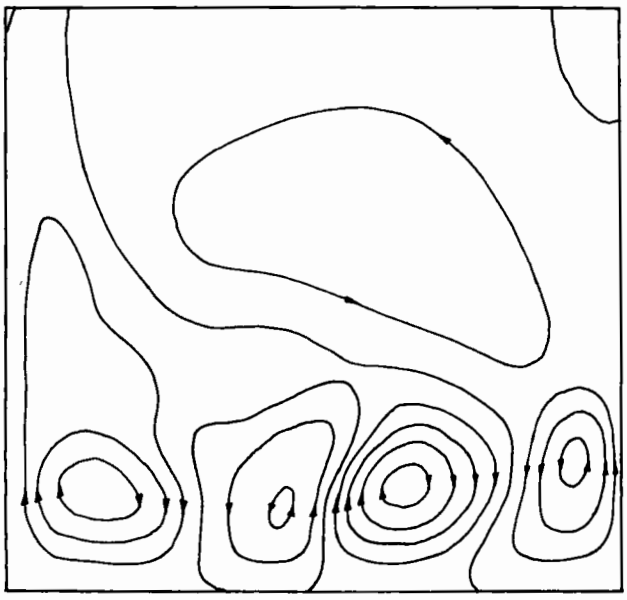

FIGURE 9. Instantaneous streamlines for case 5 ($R = 4000$, $A = 1{\cdot}0$) at $t_{bl} = 0{\cdot}346$.

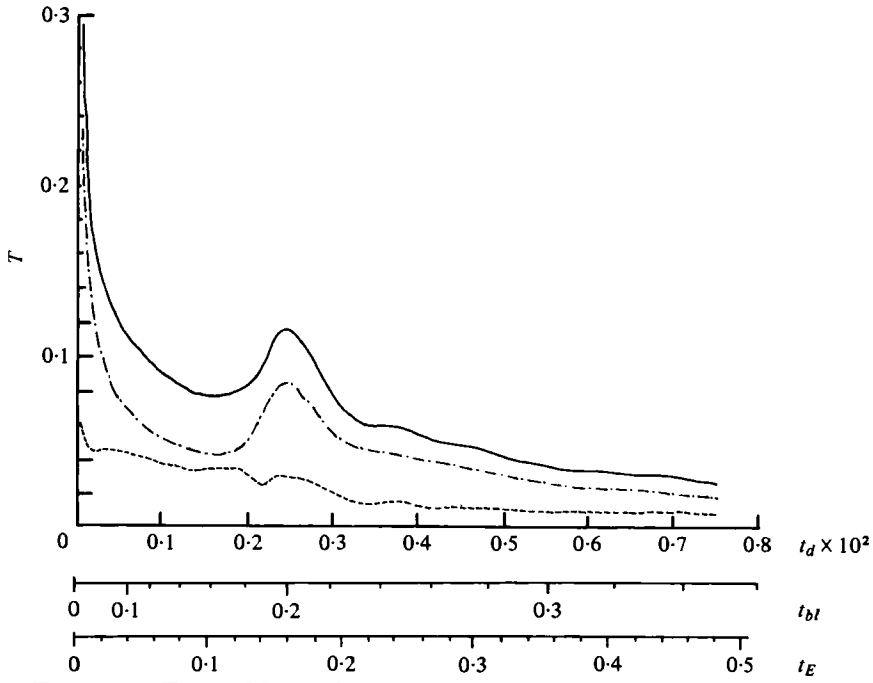

FIGURE 10. Torque history for case 5 ($R = 4000$, $A = 1{\cdot}0$). ——, T; —·—·—·, T_s; – – – –, T_e.

Case no.	A	R	t_0: t_{bl}	t_0: t_{bl} (expt.)	t_0: t_E	t_{ad}: t_{bl}	t_{ad}: t_E	Δt_E due to instab. (%)	ΔL at spin-down time (%)	L_R at onset
1	0·5	2000	0·33	—	0·64	0·35	0·67	0	0	0·12
2	1·0	1000	Stable	—	Stable	0·47	0·44	N.A.	N.A.	N.A.
3	1·0	2000	0·30	—	0·25	0·40	0·45	17	10	0·15
4	1·0	3000	0·22	—	0·16	0·36	0·45	51	17	0·09
5	1·0	4000	0·17	—	0·11	0·34	0·47	60	20	0·10
6	2·0	1000	0·52	0·36	0·28	0·57	0·32	0	0	0·19
7	2·0	2000	0·28	0·19	0·11	0·46	0·29	39	14	0·15
8	2·0	3000	0·22	0·15	0·083	0·42	0·30	62	20	0·12
9	3·0	1000	0·55	—	0·20	0·59	0·23	0	0	0·20

TABLE 1. Results for impulsive spin-down to rest. t_{bl} (expt.) is taken from Euteneuer (1972).

flow shortly after onset of centrifugal instability (which begins at the midplane). We also see modifications to the flow in the vicinity of the corner where side wall and end wall meet. Figure 7 shows a well-developed pattern of side-wall vortices of various sizes while figure 8 shows how this pattern has been evolved in time while the side-wall layer has thickened. In figure 9 the flow has spun down considerably and exhibits a much weaker and less organized vortex structure than seen in the previous figures.

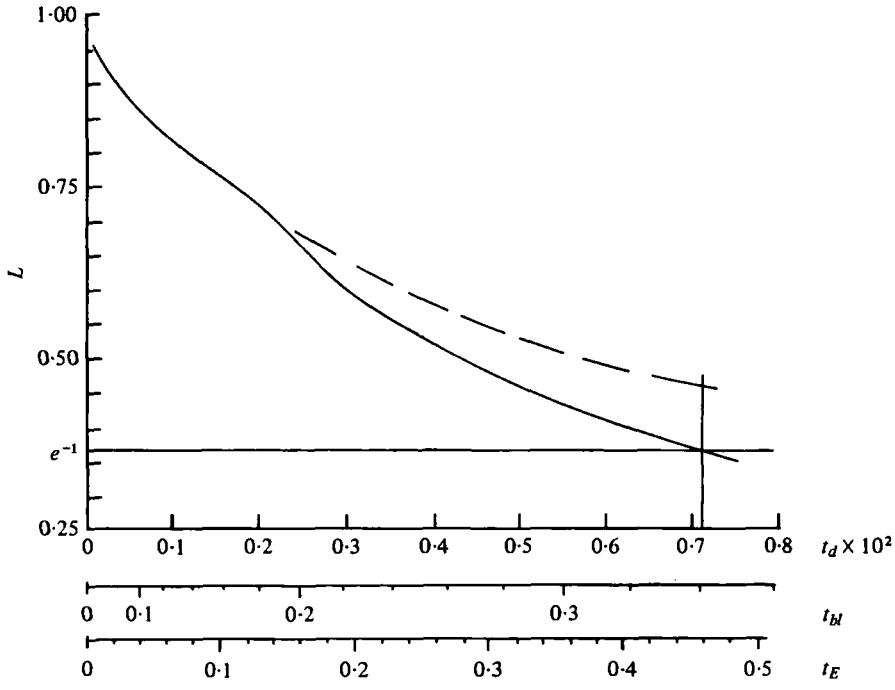

FIGURE 11. Angular momentum history for case 5 ($R = 4000$, $A = 1{\cdot}0$). ——, actual; — — — —, extrapolated 'stable' history.

The torque history for case 5 is plotted in figure 10. Shown are the total torque on the cylinder and the individual side-wall and end-wall components. The effect of the instability is apparent; the side-wall component of torque begins to increase in the vicinity of $t_{bl} = 0{\cdot}17$, indicating the *onset of instability*. This is our definition of the onset time t_0 and is presented later in table 1 for all cases considered. Notice also the dip in the end-wall torque component that accompanies the rise in T_s. This is probably due to the flow modifications which are taking place near the corner (figure 6), which is the most sensitive part of the end wall with respect to torque. This dip in the end-wall torque near the onset time was present in all cases in which instabilities were seen.

The history of the angular momentum ratio L is shown for case 5 in figure 11. The solid curve represents the calculated $L(t)$, which is a result of the spin-down flow plus the effects of the added mixing due to instability. In order to assess the effect of the latter only, one would have to subtract $L(t)$ for the spin-down flow alone. This would require a 'noiseless' numerical computation which would correspond to a physical state having no disturbances. Since we do not know how to perform such a calculation, we must be content with an extrapolation of $L(t)$ from the calculated curve from times below the onset time, as determined from $T_s(t)$, to later times. Thus, the dashed curve in figure 11 represents an estimate of the form of $L(t)$ had no disturbances been present in the system.

We define the spin-down time t_{sd} as the instant at which $L(t) = e^{-1}$. For this case it occurs at $t_{bl} = 0{\cdot}34$. Therefore, the streamlines of figure 9 correspond to those at roughly the time at which the flow has been defined to be spun down. Notice at the

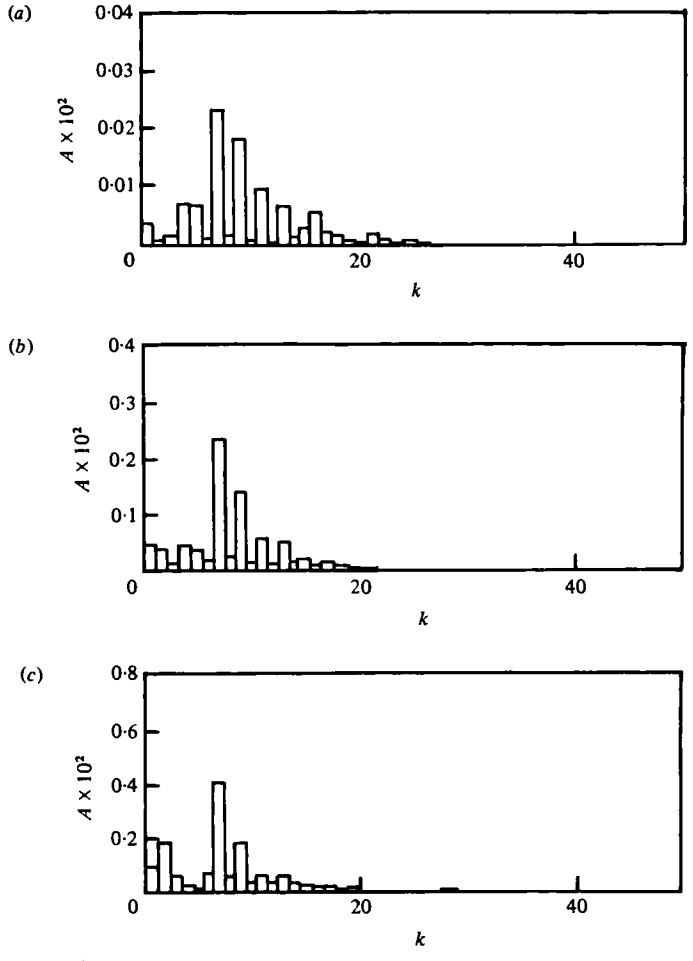

FIGURE 12. Amplitude spectra for case 5 ($R = 4000$, $A = 1{\cdot}0$) for $t_{bl} = 0{\cdot}212$. (*a*) $r = 0{\cdot}990$, (*b*) $r = 0{\cdot}954$, (*c*) $r = 0{\cdot}901$.

spin-down time that L is about 20 % smaller than the extrapolated, instability-free L would have been. This is a result of the enhanced mixing due to the presence of the Taylor–Görtler vortices. If we take the extrapolated curve seriously up to the point where it reaches the value e^{-1}, then we see that the enhanced mixing decreases the spin-down time by a factor, shown in table 1 as Δt_E, of about 60 %.

Figures 12 and 13 are plots of amplitude spectra $A(k, t)$ versus axial wavenumber k for two different times. Each spectrum was computed for three different radial positions near the side wall to see whether radial position strongly influences the results. The spectra in figure 12 show peaks at all three radial locations at values of $k = 7$ and $k = 9$ with the former wavenumber dominant. In figure 13, these components have been reduced and the dominant wavenumber is now $k = 6$. Clearly, the spectra at all radii give similar conclusions. Figures 12 and 13 correspond in time to the streamlines of figures 7 and 8 respectively and show the shift to lower wavenumbers with time. This shift is more dramatically illustrated by examining the histories

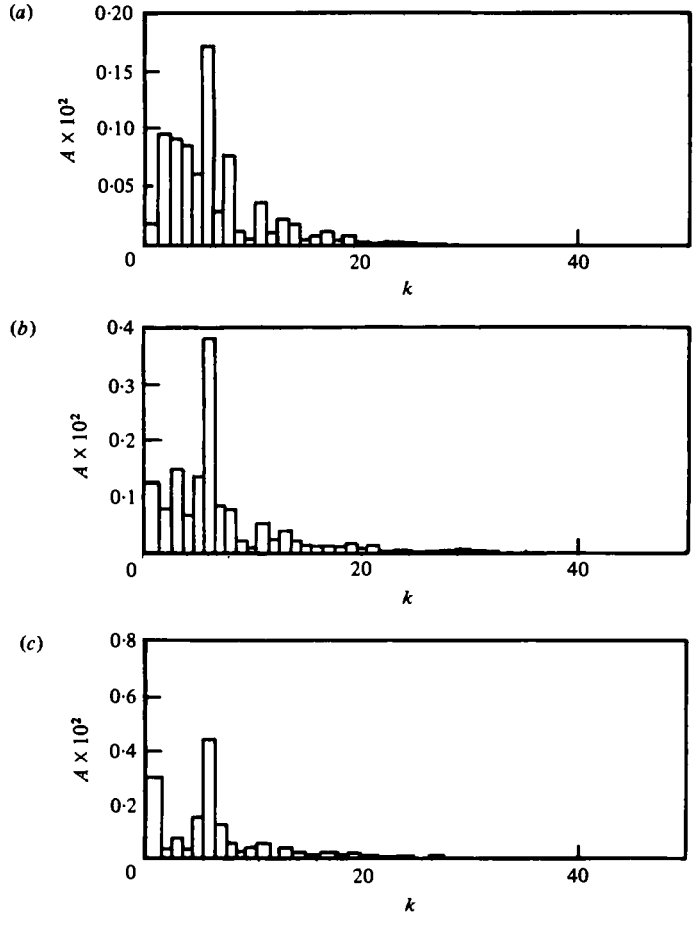

FIGURE 13. Amplitude spectra for case 5 ($R = 4000$, $A = 1{\cdot}0$) for $t_{bl} = 0{\cdot}264$. (*a*) $r = 0{\cdot}954$, (*b*) $r = 0{\cdot}901$, (*c*) $r = 0{\cdot}857$.

of neighbouring wavenumbers. This is shown in figure 14, where amplitude histories of the $k = 5$, 6, and 7 components of the spectrum at $r = 0{\cdot}990$ are plotted. The shift in dominant wavenumber from 7 to 6 and later to 5 is readily apparent.

Figure 15 is a plot of Rayleigh length, L_R, versus time for case 5. L_R is positive for all time, indicating inviscid instability in a quasi-steady sense. The behaviour typical of cases which experienced instability is that of oscillatory behaviour of L_R followed by a large drop in the vicinity of the onset time. This is seen in figure 15 with the early oscillations being weak. The previously determined onset time is indicated. The roughness of the curve for late times is partially due to the fact that not every time step was stored on the disc during the Navier–Stokes computations.

An additional remark must be made with respect to the use of the Rayleigh criterion. Equation (3.4) may be useful as an indicator of possible swirl flow instability when applied to a pure basic state without disturbances. Since, in these computations, it is impossible to separate the basic state from the disturbed state, we must disregard

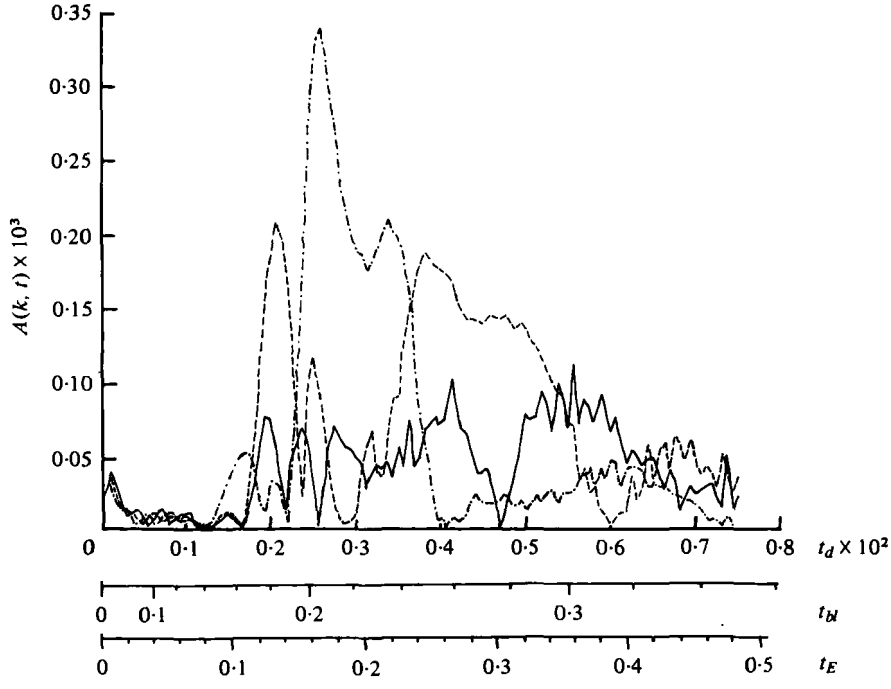

FIGURE 14. Spectral histories for case 5 ($R = 4000$, $A = 1{\cdot}0$) for $r = 0{\cdot}990$. ——, $k = 5$; — — — —, $k = 6$; —·—·—·, $k = 7$.

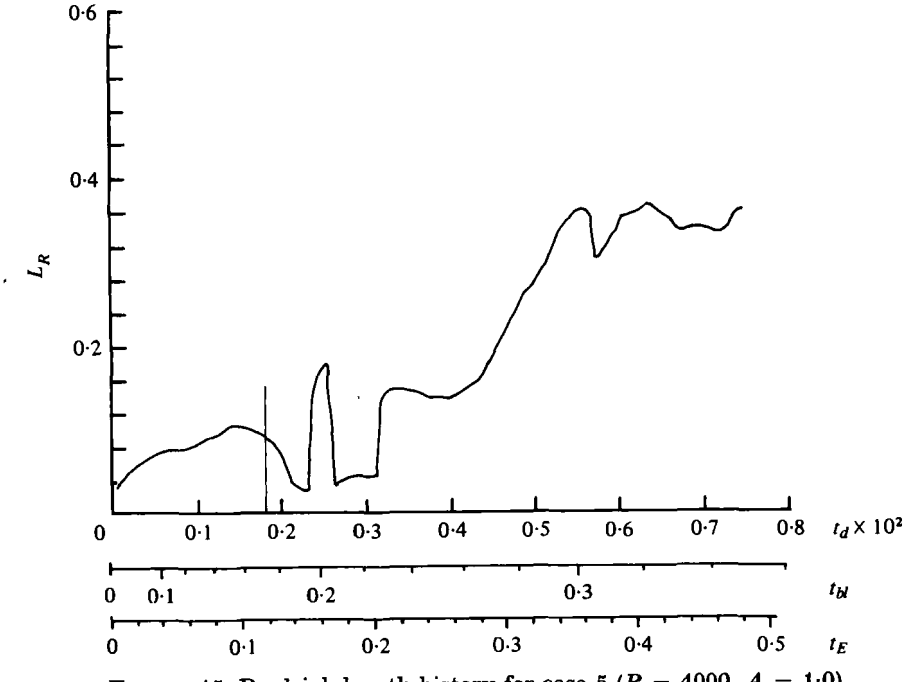

FIGURE 15. Rayleigh length history for case 5 ($R = 4000$, $A = 1{\cdot}0$).

the Rayleigh length computation for times after which we are certain that the onset of instability has occurred.

We now turn to the results of the calculations shown in table 1. This is a summary of nine numerical experiments in the ranges $0{\cdot}5 \leqslant A \leqslant 3{\cdot}0$ and $1000 \leqslant R \leqslant 4000$. We show the onset times (defined by the side-wall torque T_s), and the spin-down times (defined by the angular momentum L) in terms of t_{bl} and t_E; t_d is directly related to t_{bl} through relation (3.10*a*). Further, we indicate L_R at onset as well as Δt_E, *the percentage decrease in the spin-down time as a result of the Taylor–Görtler vortices*, and ΔL, *the percentage decrease in angular momentum at the spin-down time.*

Case 2, in which $A = 1{\cdot}0$, $R = 1000$, showed no tendency toward instability. All other cases led to well-developed Taylor–Görtler vortices as indicated.

Onset times. The onset times decrease with increasing Reynolds number for fixed aspect ratio consistent with the results of Euteneuer (1972). This is seen by examining cases 3–5 or 6–8.

The experimental values, which appear in table 1 for cases 6–8, were estimated from the wavelength *versus* time curves of Euteneuer (1972) by assuming that the earliest appearing point on each curve corresponds to the onset time. That the experimental values lie about 30 % below those predicted numerically could be due to the experiment having larger disturbances than our numerical simulation, in which case an earlier instability might result. Furthermore, our simulation excludes non-axisymmetric (e.g. Ekman layer) instabilities that might trigger the experimentally observed flows. However, we know of no observations that support the existence of such effects.

It appears, if one uses the boundary-layer time scale, that the onset time is relatively insensitive to the aspect ratio A for a given R. This is seen by examining cases 1, 3 and 7, cases 4 and 8 or cases 6 and 9. We thus see that the side-wall boundary layer is centrifugally unstable, the instability depends on the local structure of the boundary layer and very weakly on the overall spin-down flow. This is in part due to the onset of instability occurring before the spin-down mechanism is effective.

A technique which has been used to correlate experimentally determined onset times (Tillmann 1967, Maxworthy 1971; Weidman 1976*b*) involves applying a Görtler criterion to instantaneous sidewall velocity profiles. This quasi-steady stability approach results in a constant value for a parameter G_θ, where

$$G_\theta = R(\theta/a)^{\frac{1}{2}}, \tag{4.1}$$

and θ is the momentum thickness of the side-wall layer. Tillmann (1967) defines θ (in our notation) as

$$\frac{\theta}{a} = \frac{(2^{\frac{1}{2}}-1)}{2\pi^{\frac{1}{2}}}\, t_{bl}. \tag{4.2}$$

The values of G_θ calculated for cases 1–9 using equations (4.1) and (4.2) range from 11·2 to 16·3. Furthermore, our neat characterization of t_0 depending principally on R and only weakly on A is submerged using the parameter G_θ. Hence, there seems to be little advantage in using a Görtler criterion to correlate our numerical results. Likewise, such a correlation seems ineffective in understanding the three experimental points of Euteneuer listed in table 1. It is probably the quasi-steady nature of the Görtler criterion that makes it invalid quantitatively in the present spin-down cases.

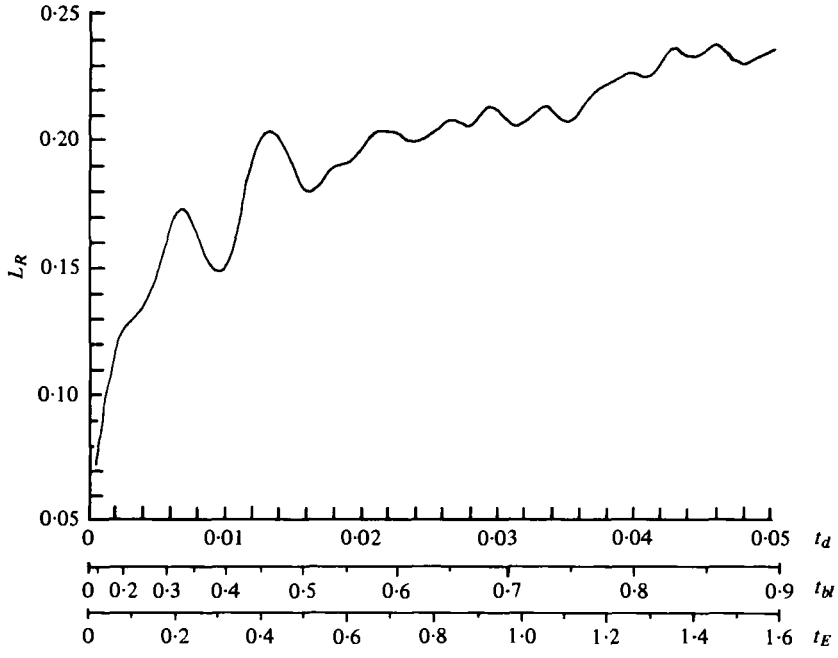

FIGURE 16. Rayleigh length history for case 2 (R = 1000, A = 1·0).

Spin-down times and spin-down augmentation. The spin-down times are relatively insensitive to Reynolds number changes for fixed aspect ratio when measured in terms of the Ekman time scale, while it increases with aspect ratio for a given Reynolds number. We thus see that the spin-down rate continues to be controlled by the Ekman blowing from the end-wall layers (as long as A is not too large) since the spin-down continues to be scaled with t_E. However, there is substantial enhancement of spin-down due to the Taylor–Görtler vortices. This may be seen by examining the columns of table 1 labelled Δt_E and ΔL, which estimate the effect of the instability on the spin-down process.

Δt_E is an estimate of the percentage decrease in spin-down time due to the presence of Taylor–Görtler vortices. It was computed by extrapolating the angular momentum trend prior to the onset time, determining the 'stable flow' spin-down time from this extrapolated curve, and then relating this to the calculated spin-down time. Cases 1, 6 and 9 show a value of zero even though they experienced instability. An examination of onset and spin-down times for these cases reveals that this is due to the fact that onset occurred just slightly before the flow was defined to be spun down. Hence, the instability played little, if any, part in the spin-down process for these cases. For those cases (3–5, 7–8) where onset occurs significantly before the spin-down time, the enhanced mixing due to the vortices brings about significant reductions in the spin-down time. These vary from 17 % for case 3 to 62 % for case 8. For a fixed aspect ratio these values of Δt_E increase with Reynolds number due to the fact that the onset of instability occurs earlier in the overall process, thus giving the vortices a longer time to contribute. Obviously, since these values are computed from data extrapolated over sometimes large distances, they cannot be considered accurate in a quantitative

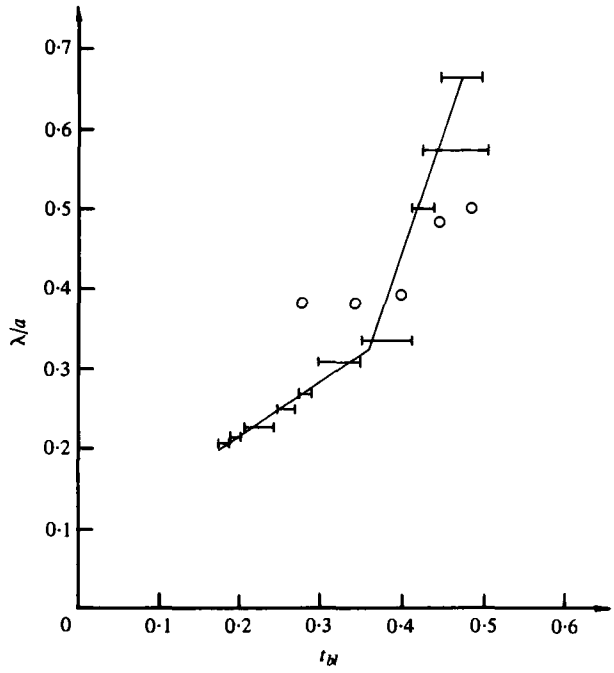

FIGURE 17. Comparison of case 7 (R = 2000, A = 2·0) results with Euteneuer (1972) data for disturbance wavelength. ——, Euteneuer (1972); ○, present numerical experiment.

sense. However, they are useful in qualitatively assessing the efficiency of the instability mechanism for various Reynolds number/aspect ratio combinations.

The column labelled 'ΔL at spin-down time' was also computed using the extrapolated angular momentum history. ΔL is an estimate of the percentage decrease in angular momentum at spin-down due to the instability. ΔL ranges from 10 % for case 3 to 20 % for cases 5 and 8. The same trends discussed with respect to Δt_E are found here. In this case, however, one has more confidence in the quantitative accuracy of the results since the required extrapolation (only up to the actual spin-down time) is not as severe.

Rayleigh lengths. The value of the Rayleigh length L_R just prior to the dip characteristic of the onset of instability has values that fall in the range $0{\cdot}09 \leqslant L_R \leqslant 0{\cdot}20$. However, a value of L_R in this region is not a sufficient condition for instability, as can be seen from figure 16 (case 2), where the value of L_R rises to nearly 0·24, but no instability was seen. Thus, the Rayleigh criterion, when applied in this manner, seems to be a poor indicator of instability for this type of unsteady, viscous, three-dimensional flow.

Comparison with experiment. The experiments of Euteneuer (1972) allow comparison with two of the cases considered in this study. Euteneuer's primary concern was the evolution of vortex wavelength with time. He measured the average wavelength from photographs of the flow (vortices were made visible using aluminium flakes). As noted earlier, neither the computations nor the experiments yield unique vortex sizes at any time, but rather show a range of wavelengths. Euteneuer observed that the wavelength increased more or less linearly with the boundary-layer time scale, but

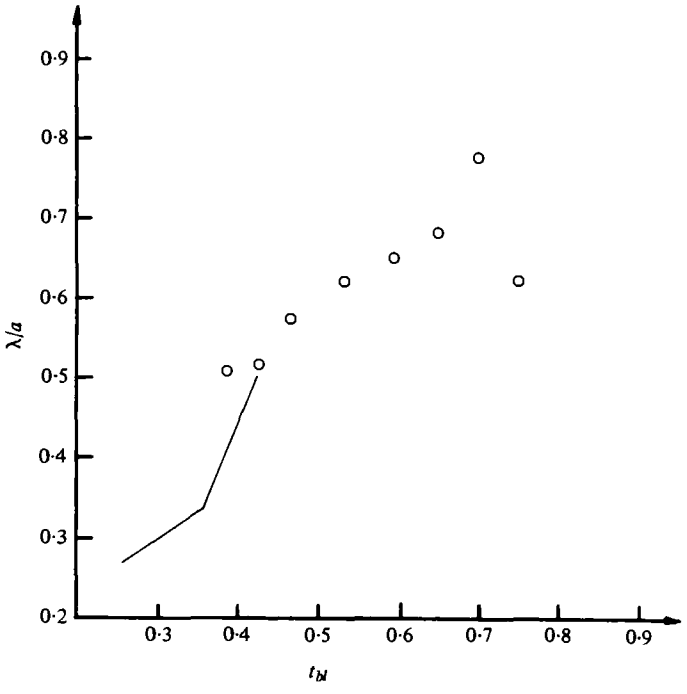

FIGURE 18. Comparison of case 6 (R = 1000, A = 2·0) results with Euteneuer (1972) data for disturbance wavelength. ——, Euteneuer (1972); ○; present numerical experiment.

that after a certain 'knee-point' a change in slope was observed. Actually, the change in wavelength is not smooth, but occurs in a step-wise fashion as vortices coalesce to adjust to the changing side-wall boundary layer. This fact can be observed in figure 17, where Euteneuer's actual data are represented by horizontal lines with vertical end bars.

For the purpose of comparison with Euteneuer's data, average wavelengths were computed 'visually' from the contour plots of instantaneous streamlines. For cases 6 and 7 this was done by counting the number of vortex pairs and dividing this number into the length of the cylinder covered by the instability.

For case 6, the results are shown in figure 18. The quantity λ/a is the vortex pair wavelength scaled on cylinder radius. The agreement for this case is only fair. This could be due to the fact that the instability is very weak. In fact, this is the lowest Reynolds number (1000) for which Euteneuer (1972) has displayed any data. This *may* indicate that for lower Reynolds numbers Euteneuer did not observe any instability at all, a result which would not be inconsistent with the fact that our instability for this case was extremely weak.

For case 7 (figure 17) the agreement is reasonably good and the sharp increase in Euteneuer's data coincides roughly with a similar increase in the numerical experiment results. For large times, however, the results of the numerical computations must at least be suspect because of the assumptions of axisymmetry and midplane symmetry. Experimental evidence (Greenspan 1968, figure 6.3; Innes 1973) seems to

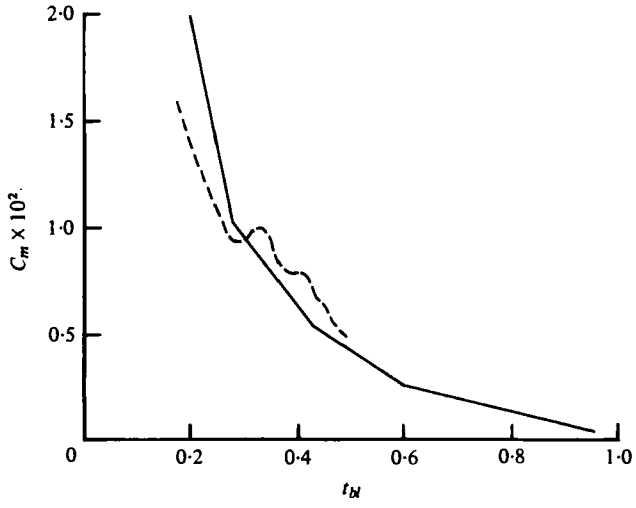

FIGURE 19. Comparison of case 7 ($R = 2000$, $A = 2{\cdot}0$) results with Michaelidis (1977) data for torque ($C_m = (\pi A)^{-1} T$). ——, Michaelidis (1977) with $3{\cdot}5 \leqslant A \leqslant 5{\cdot}0$; — — — —, present numerical experiment with $A = 2{\cdot}0$.

indicate that, while the initial vortices may indeed be axisymmetric, they do not remain so for long.

Figure 19 gives a comparison between the torque computations for case 7 and the experimental torque measurements of Michaelidis (1977). The first break in Michaelidis' data occurs at approximately the same location as Euteneuer's *Knickstelle*. The results of the numerical experiment also show a wiggle at the same point. One point that makes comparison difficult is that the aspect ratio of the cylinder used by Michaelidis is not stated. No mention of it could be found in the 1977 paper, and his doctoral dissertation states only that cylinders in the range $3{\cdot}5 \leqslant A \leqslant 5{\cdot}0$ were used. Higher aspect ratios would tend to give higher values of T_s for early time due to the increased size of the side wall. In light of the violently unsteady nature of the flow during impulsive spin-down and the assumptions of axisymmetry and midplane symmetry made by the Navier–Stokes computation, the agreement with experiment for case 7 is felt to be very good.

The results of figure 19 relate to Euteneuer's conjecture that the Knickstelle results from a Tollmien–Schlichting (T-S) instability mechanism. If one believes that the wiggle in the torque curve from the numerical experiment corresponds to the Knickstelle in the data, then a T-S mechanism is excluded since the computations are for axisymmetric modes. On the other hand a photograph in Euteneuer (1972) shows vortices for a time after the Knickstelle that are seemingly turbulent. If this is the case, secondary (non-axisymmetric) instabilities must be present and these could well result from a T-S instability.

A word should be mentioned about how the present work impinges on the original motivation of the work, viz. the possibility that spin-down instabilities may be important in the dynamic instability of liquid-filled shells. The best 'fit' for the angular velocity history for the spinning down shell is exponential in time, $\omega(t) = \Omega \exp(-\alpha t)$, rather than impulsive. Selected calculations for this case were

performed by Neitzel (1979), where it was found that the coefficient α is so small that spin-down instabilities are in fact unlikely to be present even though the Reynolds numbers R based on Ω can be as high as 10^7.

G.P.N. would like to thank his former employer, the U.S. Army Ballistic Research Laboratory (B.R.L.), for support received under the long-term, full-time study programme. S.H.D was supported by the Army Research Office under Grant no. DAAG-29-79-G-0030. Both authors wish to thank Dr C.W. Kitchens of B.R.L. for his assistance with the Navier–Stokes program and Miss J.M. Bartos, also of B.R.L., for some final computations.

REFERENCES

Briley, W. R. & Walls, H. A. 1971 A numerical study of time-dependent rotating flow in a cylindrical container at low and moderate Reynolds numbers, *Proc. 2nd Int. Conf. Numer. Meth. Fluid Dyn.* Lecture Notes in Physics, vol. 8, p. 377. Springer.

Davis, S. H. 1971 Finite amplitude instability of time-dependent flows. *J. Fluid Mech.* **45**, 33.

Euteneuer, G.-A. 1969 Störwellenlängen-Messung bei Längswirbeln in laminaren Grenzschichten an konkav gekrümmten Wänden. *Acta Mech.* **7**, 161.

Euteneuer, G.-A. 1970 Einige Ergebnisse experimenteller Untersuchungen an instationâren Görtler-Taylor-Wirbeln. *Z. angew. Math. Mech.* **50**, 177.

Eufeneuer, G.-A. 1972 Die Entwicklung von Längswirbeln in zeitlich anwachsenden Grenzschichten an konkaven Wänden. *Acta Mech.* **13**, 215.

Euteneuer, G.-A., Heynatz, T. J., and Siedenkersting, H. 1968 Der Bodeneinfluss bei Anlauf- und bei Bremsströmungen zäher Flüssigkeiten in rotierenden Zylindergefässen. *Z. angew. Math. Mech.* **48**, 190.

Greenspan, H. P. 1968 *The Theory of Rotating Fluids.* Cambridge University Press.

Greenspan, H. P. & Howard, L. N. 1963 On a time-dependent motion of a rotating fluid. *J. Fluid Mech.* **17**, 385.

Innes, G. 1973 An experimental study of the Ekman layer in a contained rotating fluid. preprint.

Kitchens, C. W. 1980 Navier-Stokes solutions for spin-up in a filled cylinder. *A.I.A.A.J.* **18**, 929.

Maxworthy, T. 1971 *Turbulence Measurements in Liquids* (ed. G. K. Paterson & J. L. Zakin), p. 32. Dept. Chem. Eng., Univ. Missouri-Rolla.

Michaelidis, K. 1977 Reibungsmomente der instationären Bremsströmung am Zylindermantel eines flüssigkeitsgefüllten zylindrischen Gefässes. *Acta Mech.* **26**, 1.

Neitzel, G. P. 1979 Centrifugal instability of decelerating swirl-flow within finite and infinite circular cylinders. Ph.D. dissertation, The Johns Hopkins University.

Neitzel, G. P. & Davis, S. H. 1980 Energy stability theory of decelerating swirl flows *Phys. Fluids* **23**, 432.

Rayleigh, Lord 1916 On the dynamics of revolving fluids. *Scientific Papers*, vol. 6, 447. Cambridge University Press.

Tillmann, W. 1967 Development of turbulence during the build-up of a boundary layer at a concave wall. *Phys. Fluids Suppl.* **10**, 108.

Wedemeyer, E. H. 1964 The unsteady flow within a spinning cylinder. *J. Fluid Mech.* **20**, 383.

Weidman, P. D. 1976*a* On the spin-up and spin-down of a rotating fluid, Part 1. Extending the Wedemeyer model. *J. Fluid Mech.* **77**, 685.

Weidman, P. D. 1976*b* On the spin-up and spin-down of a rotating fluid, Part 2. Measurements and stability. *J. Fluid Mech.* **77**, 709.